The submitted manuscript has been authored by a contractor of the U. S. Government under contract No. W-31-109-ENG-38. Accordingly, the U. S. Government retains a nonexclusive, royalty-free license to publish or reproduce the published form of this contribution, or allow others to do so, for U. S. Government purposes.

CONF-850819--7

ANL-HEP-CP-85-60

ANL-HEP-CP--85-60

DE85 018448

Study of Quark Fragmentation in e^+e^- Annihilation at 29 GeV: Charged Particle Multiplicity Distributions

M. Derrick, P. Kooijman, J.S. Loos, B. Musgrave,
L.E. Price, J. Schlereth, K. Sugano, J.M. Weiss[a], D.E. Wood[b]
Argonne National Laboratory, Argonne, IL 60439

G. Baranko, P. Baringer, D. Blockus, B. Brabson, S.W. Gray[c], C. Jung,
H. Neal, H. Ogren, D.R. Rust, M. Valdata-Nappi[d]
Indiana University, Bloomington, IN 47405

C. Akerlof, G. Bonvicini, J. Chapman, D. Errede, N. Harnew[e],
P. Kesten, D.I. Meyer, D. Nitz, A.A. Seidl[b],
R. Thun, T. Trinko[b], M. Willutzky
University of Michigan Ann Arbor, MI 48109

S. Abachi, I. Beltrami, B.G Bylsma, R. DeBonte, K.K. Gan,
D. Koltick, F.J. Loeffler, E.H. Low, R.L. McIlwain, D.H. Miller,
C.R. Ng, L.K. Rangan, E.I. Shibata
Purdue University West Lafayette, IN 47907

B. Cork
Lawrence Berkeley Laboratory, Berkeley, CA 94720

MASTER

ABSTRACT

This paper presents the charged particle multiplicity distributions for e^+e^- annihilation at $\sqrt{s} = 29\ GeV$ measured in the High Resolution Spectrometer. The data, which correspond to an integrated luminosity of 185 pb^{-1}, were obtained at the e^+e^- storage ring PEP. The techniques used to obtain the original distributions from the observed prong numbers are discussed. The multiplicity distribution of the charged particles with a two jet selection has a mean value $< Nch >= 13.02 \pm 0.03 \pm 0.5$; and a dispersion $D = 3.84 \pm 0.02 \pm 0.1$. The mean multiplicity increases with the event sphericity. No correlation is observed between the multiplicities in the two jets that characterize most of the events. For the single jets a value of $D = 2.71 \pm 0.02 \pm 0.06$ is measured which gives further support the idea of independent jet fragmentation. When compared with e^+e^- data at other energies, the multiplicity distributions exhibit the scaling behavior in the mean first suggested by Koba, Nielsen and Olsen (KNO). The KNO distribution in the central rapidity interval is broader than that for the whole rapidity span and agrees well with the generalized Bose-Einstein formula for three independent sources.

DISTRIBUTION OF THIS DOCUMENT IS UNLIMITED

INTRODUCTION

The e^+e^- annihilation process at high energies leading to hadronic final states is considered to go by the initial formation of a $q\bar{q}$ pair which evolves into a *parton shower* of quarks and gluons and which subsequently fragment into jets of hadrons. We have previously presented results on the global properties of these jets[1]. In this paper the studies are extended to the multiplicity distributions of the stable charged particles produced. The multiplicities of identified hadrons (π, K, p, Λ) are given in a separate publication[2].

The multiplicity distributions provide important constraints that must be reproduced by the various fragmentation models. They may also illuminate the basic annihilation process. One clue is provided by the scaling in the mean that characterizes all high energy processes. The data on quark fragmentation is also needed to compare to the results when the initial parton is a hard gluon; some simple differences are expected[3].

Although the experimental signature of the charged multiplicity is simple, the limitations of the tracking system means that important corrections are needed. The techniques use to make these corrections are discussed. The results are compared to previous measurements of e^+e^- annihilation and to results from hadronic interactions.

APPARTUS

The data come from the hadronic annihilation events collected by the High Resolution Spectrometer (HRS) at the SLAC e^+e^- storage ring PEP. The experiment was done at a center of mass energy of $\sqrt{s} = 29\ GeV$ and the data sample corresponds to an integrated luminosity of 185 pb^{-1}.

The HRS[4], shown in Fig. 1, measures charged secondary particles over a solid angle of $\sim 90\%$ of 4π covering the angular range $|cos\theta| < 0.9$ where θ is the angle with respect to the positron beam direction. The main drift chamber

system, which is used in this analysis, consists of 15 layers of drift cells; in seven of the layers the wires are oriented axially, in the remaining eight layers they are at stereo angles of ± 60 mr. There are 2448 cells in this tracking chamber.

At a radius of 1.98m the turning angle of the tracks is measured in a two layer outer drift chamber system. The vacuum pipe of PEP and the inner cylinder of the drift chamber vessel are made of beryllium so that there is typically 1.3% of a radiation length of material between the interaction point and the first tracking layer of the detector[5]. This thin front end combined with the high solenoidal magnetic field of 16.2 kG means that additional tracks resulting from photon conversion are minimal.

The tracking system is surrounded by a set of barrel and endcap shower counters consisting of lead-scintillator sandwiches with one layer of proportional wire chambers to measure the position of the showers. A set of Cerenkov counters are located between the inner drift chamber and the outer tracking and shower detection system. The signals from these counters are not used in the present analysis.

The detector was triggered by requiring the presence of either three or more charged tracks or two charged tracks plus a signal in time with the beam crossing. Two neutral triggers were also used[1,4].

DATA SELECTION

To select the hadronic events for this study several cuts were applied to the raw data sample. The number of reconstructed tracks was required to be greater than five and less than 40. This cut removes almost all events of the reaction $e^+e^- \rightarrow \tau^+\tau^-$. To remove the few events in which both taus decay into three charged prongs, the three particle effective mass was required to be greater than 2 GeV for the six prong events of the 3-3 topology. The sum of the charged particle momenta plus the energy registered in the barrel shower counter was required to be greater than 13 GeV. These energy requirements effectively remove all events

induced by a two photon process.

To ensure good tracking efficiency, the events were restricted to be near the equatorial plane of the detector. Specifically, the thrust axis of the event was required to be more than 60^0 and less than 120^0 from the beam direction; where the thrust T was defined using the charged particles as:

$$T = max \frac{\sum_i |P_L^i|}{\sum_i P^i}$$

In addition, the individual tracks were required to have a dip angle of more than 24^0. No track was required to reconstruct in the outer drift chamber system. These cuts resulted in a data sample of 26,397 events. In addition to this inclusive data set, a sample of two jet events was selected using the sphericity (S) and aplanarity (A) variables. As in our previous study[1] the collimated ($S \leq 0.25$) and planar ($A \leq 0.10$) events are called two jet. These additional cuts, which exclude the events with hard gluon radiation, reduces the data sample to 20,600 events.

DETECTOR SIMULATION

The experiment has been simulated in a Monte Carlo (MC) program. This program has two parts; an event generator and the detector simulation. The output from the MC consists of wire hits and drift times and shower counter pulses in the same format as the real data. Such simulated events are then passed through the same reconstruction programs as the data. From the ratio of the number of generated MC events to the reconstructed MC events a series of correction factors were calculated that were then applied to the observed data. The MC event generator used in this analysis was that given by the Lund model[6]. Since we only use this simulation to produce correction scale factors, the detailed absolute agreement between the MC predictions and the data is not essential: the agreement is in fact quite good in the many comparisons that we have made. A comparable number of MC events were used as in the data.

Since this study reports charged particle multiplicities, it depends critically on a good understanding of the response of the drift chamber system to the events. After the charged tracking has been completed, a final cleanup was done. This operation consisted of three major parts, eliminating: 1) tracks considered to be spurious due to low quality, 2) tracks which appear to be duplicates of other, better tracks, and 3) tracks which appear to be made up of fragments of several other, better tracks. The final cleanup step allows rather tighter cuts on track quality than is possible during the initial track finding and reconstruction. In the initial tracking, the track candidates change and develop and the looser cuts help to define better orbits. These orbits may preclude the use of certain drift chamber coordinates in defining additional tracks. In addition, the techniques used to reject of duplicate tracks are more efficient when the event is complete.

These procedures were tuned using data; initially the sample of two prong Bhabha scattering events and then the $D^{*+} \rightarrow D^{o}\pi^{+}$ events which are cleanly tagged by the excellent spectrometer resolution and the limited kinematics available to the bachelor pion.

These measurement as well as our studies[7] of other low multiplicity final states such as $\mu^{+}\mu^{-}$ and $\tau^{+}\tau^{-}$ show that the track reconstruction efficiency for isolated tracks is greater than 99% and uniform for $\cos\theta < 0.8$. A futher test was made using the multihadron events generated by the MC program. This study was done statistically using the large MC event sample by comparing "tracking efficiency" evaluated in two different ways. The first method simply calculated the number of charged tracks reconstructed versus the number originally generated, in the two dimensional space of $|\vec{p}|$ vs $\cos\theta$ where $|\vec{p}|$ is the absolute 3-momentum and θ is the polar angle of the orbit tangent with respect to the beamline at the point of closest approach. The second method involved the calculation of the same quantities with the additional constraint that the reconstructed orbits survived a mappingback onto the original MC generated tracks via the list of drift chamber coordinates employed in the track fitting and simulation. The two methods yielded good agreement only after the final track cleanup operations.

The accidental loss of real tracks was found to be small.

Typical results of these studies are shown in Fig. 2 which gives the reconstruction efficiency for different momentum intervals as a function of the θ. For $\theta > 30°$ and p> 200 MeV/c the track *reconstruction* efficiency is 80% or better and varies slowly with angle. For p>2 GeV/c the efficiency is about 90%. Low momentum tracks (p < 200 MeV/c) are not well reconstructed for any dip angle because of the high magnetic field of the spectrometer.A track with $p \lesssim 240$ MeV/c spirals within the main drift chamber system

RESULTS

i. Multiplicity Distributions

The true multiplicity distribution is obtained from the observed distribution by using a matrix unfold technique. We assume:

$$\begin{pmatrix} N_0 \\ N_2 \\ N_4 \\ \vdots \end{pmatrix}_T = \begin{pmatrix} \alpha_{00} & \alpha_{01} & \alpha_{02} & \alpha_{03}\cdots \\ \alpha_{20} & \alpha_{21} & \alpha_{22} & \alpha_{23}\cdots \\ \alpha_{40} & \alpha_{41} & \alpha_{42} & \alpha_{43} \\ \vdots & \vdots & \vdots & \vdots \end{pmatrix} \begin{pmatrix} N_0 \\ N_1 \\ N_2 \\ N_3 \\ \vdots \end{pmatrix}_O$$

where N_{2T}, for example, is the number of true two prong events and N_{20} is the number of two prong events observed in the detector after reconstruction. The true distribution contains only even numbers of prongs whereas the observed distribution has about the same number of events with an odd number of prongs as an even number of prongs because of the losses (and gains) in the tracking process.

For the lower multiplicities the observed distribution is only slightly shifted from the generated number as shown in the calculated frequency distribution of the true eight prong events in Fig. 3. For the higher multiplicities the smearing is much more important: the peak of the reconstructed 16 prong events, also shown in Fig. 3, occurs at 12 prongs and extends as low as 8 prongs.

The charged particle multiplicity distribution for the two jet sample that results from this unfolding process is given in Table I and is shown in Fig. 4. Table II gives the $< Nch >$ and dispersion value that characterize this distribution. The first error is statistical and the second systematic.

Since the results are based on a large data sample, the errors are primarily systematic and come mainly from the uncertainties in the MC simulation of the tracking process. To estimate the size of these errors, the analysis was repeated cutting the data into several smaller samples. In particular, since the spectrometer was operated over a three year period with a somewhat different complement of detectors, the data collected in the first year (20 pb^{-1}) when no Cerenkov counters were installed, during the second year (91 pb^{-1}) when the vertex chamber was not in place and the third year (74 pb^{-1}) were analysed separately.

In addition, the analysis was repeated varying the cut on the dip angle of the thrust axis and on the fraction of potential drift chamber hits required for a track candidate. The resulting systematic errors are typically 5%. For the events with Nch = 2 and Nch = 4 that are removed by the initial cut, we depend on the MC simulation. Since, as we discuss later, the q and $\bar{q}$ fragment independently the data also measures the number of such events. For example, the probability of having a 3 prong jet is measured in the 3-8 events (say) even though the 3-1 events, that are a part of the four prong event sample, are removed by the cut.

In the MC event generation, initial state electromagnetic radiation is included so that the mean center of mass energy is 27.3 GeV. The corrections for external and internal pair conversions have also been made. They are small and typically reduce $< Nch >$ by 0.1.The charged particles resulting from heavy particle decay such as $D^o \rightarrow K^-\pi^+, K^o \rightarrow \pi^+\pi^-$and $\Lambda \rightarrow p\pi^-$ are included. The latter two decays are usually omitted when quoting results from hadronic interactions. The multiplicities[2] of $< N_{K^o} >= 1.51 \pm 0.05 \pm 0.13$ and $< N_\Lambda >= 0.191 \pm 0.013 \pm 0.016$ reduces $< Nch >$ for the total data sample to $11.5 \pm 0.03 \pm 0.6$ if the charged particles from these decays are removed.

Our results are in good agreement with the trend of other e^+e^- data, both for $< Nch >$ and for D as shown in Fig. 5. The distribution in prong number also agrees with other measurements[8] as is illustrated in Fig. 6 which shows the *multiplicity distribution expressed as a function of the mean as first suggested by* Koba, Nielsen and Olesen[9] (KNO) for hadronic interactions (based on Feynman scaling and a logarithmic growth of <Nch>). Such a scaling in the mean was later found to characterize multiplicity distributions from all high energy interactions of a given type including hadronic scattering, deep inelastic lepton scattering and e^+e^- annihilation[10].

If $z = Nch/ < Nch >$ then KNO scaling says that:

$$\psi(z) =< Nch > \frac{\sigma_n}{\Sigma\sigma_n} \tag{1}$$

where $\psi(z)$ is a universal function for a given type of reaction and σ_n is the cross section for the production of the final state containing n charged particles.

The comparison of high energy e^+e^- data shown in Fig. 6 that spans the range from $\sqrt{s} = 14\ GeV$ to $\sqrt{s} = 34 GeV$ shows that this scaling holds well. This distribution is significantly narrower than pp data in the same energy range and this difference is not a result of the diffractive component in the latter as can be seen in Fig. 7 where the HRS e^+e^- data is shown compared to the power low fit to the non-diffractive pp data (dashed line) of:

$$\psi(z) = e^{-3.5z}(-2.72z + 75.9z^3 - 16.35z^5 + 0.89z^7) \tag{2}$$

The KNO scaling of the hadronic data is observed up to $\sqrt{s} \sim 60\ GeV$ but at 540 GeV, the energy of the CERN $\bar{p}p$ collider, the scaling breaks down. Many more high multiplicity events are observed than are predicted from the KNO fit to lower energy data[11]. In addition, the multiplicity distributions for selected pseudo rapidity ($\eta = -\ell n\ tan\ \theta/2$) ranges differ, with the central region $|\eta| < 0.5$ showing an almost exponential fall off being represented by:

$$\psi(z) \sim 4ze^{-2z}. \tag{3}$$

Such a qualitative difference is also seen in the HRS e^+e^- data as shown in Fig. 8 where the KNO scaling distribution is given for the central region of rapidity $|Y| \leq 1$. ($Y = -0.5\ell n\frac{E-P_L}{E+P_L}$ where P_L is the component of momentum parallel to the thrust axis).

Bialas and Hayot[12] have suggested that the broader distribution seen for the central rapidity interval arises since energy and momentum conservation supresses the higher multiplities for events in the complete rapidity span. A wider distribution for the central region is also expected just from fluctuations, since for some events the central region will be populated mainly by charged particles and for others mainly by neutral particles.

One interpretation of the KNO distribution is that it results from the superposition of k independent but identical sources[10]. For $< Nch >$larger than k the negative binomial distribution reduces to

$$\psi_k(z) = \frac{k^k}{(k-1)!}z^{k-1}e^{-kz} \tag{4}$$

which gives Eq. (3) for k=2 and

$$\psi(z) \simeq 4.5z^2e^{-3z} \tag{5}$$

for k=3. The curves corresponding to these two choices of k=2 and k=3 are shown on Fig. 8. The k=2 curve (dashed line) is broader than the data but the k=3 variation(full line) is in remarkable accord with our measurements

ii. Single Jet Multipliticies

If the events are divided into two individual jets by a plane perpendicular to the thrust axis then the multiplicity properties of single quark fragmentation can be measured. The corrections for detector resolution are done in the same way as for the full event except that now charge conservation cannot be applied to each jet individually.

The corrected multiplicity distribution for the single jets in the two jet sample with $S \leq 0.25$ and $A \leq 0.1$ is shown in Fig. 9 and is also listed in Table I. This single jet distribution has $\frac{<Nch>}{D} = 2.42 \pm 0.10$ giving an $\frac{<Nch>}{D}$ ratio to the full event of 1.36 ± 0.05 which is consistent with the idea that the distribution for the total events just results from the incoherent addition of two equal distributions since in this case the $< Nch > /D$ ratios should just differ by $\sqrt{2}$.

iii. Forward-Backward Multiplicity Correlations

A further check on this hypothesis of fragmentation independence is provided by the forward:backward (F:B) multiplicity correlations. The forward direction is defined as that jet pointing along the incident positron beam direction. The results, shown in Fig. 10(a) indicate at most a weak correlation. Since there will be correlations in rapidity coming from, for example, the decays of centrally produced resonances or the spill over of low momentum particles from one jet to the other, Fig. 10(b) shows the same F:B multiplicity correlation plot with the central region of rapidity, $|Y| < 1$, removed. A small F:B correlation is expected from the fact that the different quark flavors are always produced in pairs and that the $< Nch >$ values for the different quark flavors are slightly different[13]

When expressed in the KNO form the single jet data gives the distribution shown in Fig 11.

iv . Rapidity Distributions

The corrected rapidity distribution along the thrust axis is shown in Fig. 12(a). The distribution has a flat plateau but with a shallow dip near Y = 0. All particles are assigned the pion mass in calculating the rapidity and so any heavier particles are shifted to larger $|Y|$ values. The central dip still remains, however, after correcting for this effect[1]. Figure 12 also shows the rapidity distributions for three different multiplicity selections (b) $Nch \leq 9$ (c) $10 < Nch < 12$ and(d) $Nch \geq 13$, where Nch is the observed multiplicity. As Nch increases the distributions became narrower and the central dip is enhanced. This is consistent with the observation that much of the peaking near $|Y| \sim 2$ results from particles coming from the decay of D and B mesons containing the c and b quarks and that such events tend to have a higher multiplicity[13].

v. Sphericity Variation of $< Nch >$

The mean charged multiplicity as a function of event sphericity is shown in Fig. 13, where the sphericity is determined by the eigenvalues of the momentum tensor. The sharp rise at low sphericity comes about because events with low values of Nch give low sphericity values when the sphericity is defined from the charged particles alone. The slower rise, amounting to about 20%, in the higher sphericity region is the effect of hard gluon radiation. The full line, which is in qualitative agreement with the data, shows the prediction of the MC program. If the hard gluon emission is suppressed in the MC event generation then no such rise is predicted as seen by the dashed line. The events at high sphericity are predominantly of the three jet topology.

The rise of $< Nch >$ with sphericity, for $S \leq 0.2$ agrees with the measurements of the PLUTO collaboration[14]. The increase of $< Nch >$ for $S \geq 0.2$, due to hard gluon radation was not previously observed. This contributes to the change of slope of $< Nch >$ vs $\sqrt{s}$ seen in Fig. 5(a) above 19 GeV. Our results,

however, indicate that only a small part of this increase can be attributed to hard gluon effects.

Fig. 14 shows the KNO distribution for low ($S < 0.05$) and high ($0.5 < S < 0.7$) sphericity data; within errors the distributions scale.

DISCUSSION AND CONCLUSIONS

The charged particle multiplicity distributions presented here are in good agreement with other measurements in this energy range and show the KNO scaling that characterizes most high energy interactions. Such a scaling results from a casade process such as the tree branching at the parton level in e^+e^- annihilation[15]. The central region of rapidity gives a much wider KNO distribution similar to but again narrower than that seen in the highest energy hadronic collisions. One interpretation[16] of the latter is that the high p_T jets that characterize a significant fraction of such events are responsible for the excess of high multiplicity events. Such an explanation is not relevant to the e^+e^- data.

The single jet multiplicity distribution is wider than the total event distribution by a factor of $\sqrt{2}$ consistent with the independence of the forward and backward jets. This observation supports the suggestion of Carruthers and others[17] that the KNO scaling phenomenon is a rather general result in physics and reflects particle emission by a small number of independent sources. The distribution for the full rapidity range may be influenced by kinematic constraints and indeed the central rapidity region shows a wider distribution that is quantitatively represented by a Bose-Einstein or negative binomial distribution for three independent emitters. Whether these emitters can be associated with the quark, antiquark and gluon remains to be proved.

The effects of gluon radiation are seen in the increase of $< Nch >$ with event sphericity, although the high sphericity and low sphericity data show the same KNO distributions which does not support the idea that k=3 for such events.

The separation of a clear three jet sample and the measurement of the individual multiplicites will clarify this issue and also allow us to investigate the gluon jet multiplicity which is naively expected to be 9/4 times larger than the quark jet. The gluon jet should also show a narrower KNO distribution[3].

ACKNOWLEDGMENTS

This work was supported by the U.S. Department of Energy. We thank the PEP staff for operation of the storage ring at high luminosity.

(a) Now at SRI International, Menlo Park, CA 94025.

(b) Now at Lockheed Missiles & Space Co., Sunnyvale, CA 94086.

(c) Now at Laboratory for Nuclear Studies, Cornell University Ithaca, NY 14853.

(d) Permanent address: INFN. Pisa, Italy.

(e) Now at CERN, CH-1211 Geneva 23 Switzerland.

REFERENCES

1. D. Bender, et al., *Phys. Rev.* D31, 1 (1985).
2. M. Derrick, et al., Particle Production in e^+e^- Annihilation at $\sqrt{s}$= 29 GeV *Phys. Rev. D.*
3. M. Derrick and T. Gottschalk, Proceedings of the 1984 Summer Study on the Design and Utilization of the Superconducting Supercollider, Snowmass, Colorado.
4. D. Bender, et al., *Phys. Rev.* D30, 515 (1984).
5. For 74 pb^{-1} of data a four layer vertex tracking chamber was in operation. We do not use data from this system in the present analysis.
6. B. Andersson, G. Gustafson, G. Ingelman and T. Sjostrand, *Phys. Rep.* 97, 32 (1983). The partons are generated according to the Lund string model and are then fragmented using the Feynman and Field prescription.
7. M. Derrick, et al., *Phys. Rev.* D31, 2352 (1985), K. K. Gan, et al., *Phys. Lett.* 153B, 116 (1985).
8. M. Althoff, et al., *Z Phys.* C22, 307 (1984).
9. Z. Koba, H.B. Nielsen and P. Olesen, *Nucl. Phys.* B40, 317 (1972).
10. For a recent review see M. Derrick, "Multiplicities in High Energy Interactions", Proceedings of 1985 Aspen Winter Physics Conference, ANL HEP CP 85-17.
11. K. Alpgard, et al., *Phys. Lett.* 123B, 361 (1983)
12. A. Bialas and F. Hayot, *Phys. Rev. D.*
13. The $< Nch >$ value for single jets of (u,d,s) quarks is 5.8 $\pm$ 0.1 and for c quarks 6.6 $\pm$ 0.2. (M. Derrick, et al., ANL HEP PR 85-20). For b quarks it is 7.611 $\pm$ 0.46 (M. Sukuda, et al., (*Phys. Lett.* 152B, 399 (1984)).
14. Ch. Berger, et al., *Z Phys.* C12 297, (1982). These results are based on small data samples spanning the range $7.7 < \sqrt{s} < 31.6\ GeV$.

15. S. Ellis, Proc. of 11th SLAC Summer Institute, SLAC Report #267 (1983); B. Durand and S. Ellis, Proceedings of the 1984 Summer Study on the Design and Utilization of the Superconducting Super Collider, Snowmass, Colorado.

16. G. Panchieri, Proceedings of XV Symposium on Multiparticle Dynamics (1985).

17. P. Carruthers and C.C. Shih, *Phys. Lett.* 137B 425 (1984). *Ibid.*, 127B, 242 (1983), M. Biyajima, *Ibid.*, 137B, 225 (1984).

Figure Captions

1. The High Resolution Spectrometer
2. Mean track reconstruction efficiencies as a function of momentum (p) and dip angle (θ).
3. The reconstructed multiplicity distribution for generated 8 prong and 16 prong events according to the Monte Carlo simulation.
4. Charged Particle Multiplicitydistribution for two jet events.
5. (a) Mean Nch as a function of $\sqrt{s}$ for e^+e^- annihilation. (b) Dispersion of the multiplicity distribution for e^+e^- annihilation.
6. KNO Scaling distribution for e^+e^- annihilation.
7. KNO Scaling distribution as measured in the HRS compared non-diffractive pp data (dashed line).
8. KNO scaling distribution for e^+e^- annihilation at 29 GeV selected with $|Y| < 1$ compared to the prediction for three independent sources, k=3 (full line) and two independent sources, k=2 (dashed line).
9. Multiplicity distribution for single jets from events with S $\leq$ 0.25 and A $\leq$ 0.1.
10. Forward: backward multiplicity correlations for (a) full event (b) event with central region $|Y| < 1.0$ removed. The line shows the prediction of the Monte Carlo program.
11. KNO distribution for single jets from event with S $\leq$ 0.25 and A $\leq$ 0.1
12. Rapidity distributions relative to the thrust axis for two jet events (a) all multiplicity values (b) observed prong number Nch < 9 (c) $10 \leq Nch \leq 12$ and (d) Nch $\geq$ 13.

13. Mean charged multiplicity as a function of event sphericity. The full line shows the Monte Carlo prediction for the full event sample and the dashed line when the events with hard gluon radiation are removed.

14. KNO distribution for events with low sphericity (S< 0.05) and high sphericity 0.5 < S < 0.7.

DISCLAIMER

This report was prepared as an account of work sponsored by an agency of the United States Government. Neither the United States Government nor any agency thereof, nor any of their employees, makes any warranty, express or implied, or assumes any legal liability or responsibility for the accuracy, completeness, or usefulness of any information, apparatus, product, or process disclosed, or represents that its use would not infringe privately owned rights. Reference herein to any specific commercial product, process, or service by trade name, trademark, manufacturer, or otherwise does not necessarily constitute or imply its endorsement, recommendation, or favoring by the United States Government or any agency thereof. The views and opinions of authors expressed herein do not necessarily state or reflect those of the United States Government or any agency thereof.

TABLE I

Charged Particle Multiplicity Distributions

P(Nch) Percent		
Nch	Two Jet	Single Jet
0		0.04 ± 0.01
1		1.57± 0.06
2	0.05 ± 0.02 ± 0.05	3.55 ± 0.09
3		6.97 ± 0.13
4	0.48 ± 0.05 ± 0.20	11.00 ± 0.17
5		4.02 ± 0.20
6	3.81 ± 0.14 ± 0.20	14.64 ± 0.19
7		14.04 ± 0.19
8	10.77 ± 0.23± 0.50	11.56 ± 0.17
9		8.60 ± 0.17
10	16.88 ± 0.29 ± 0.80	5.64 ± 0.12
11		3.78 ± 0.10
12	21.23 ± 0.32 ± 1.00	2.21 ± 0.07
13		1.26 ± 0.06
14	18.18 ± 0.20 ± 0.40	0.65 ± 0.04
15		0.28 ± 0.03

TABLE I (continued)

Charged Particle Multiplicity Distributions

P(Nch) Percent		
Nch	Two Jet	Single Jet
16	13.55 ± 0.26 ± 0.70	0.12 ± 0.02
17		0.03 ± 0.02
18	8.14 ± 0.20 ± 0.40	0.03 ± 0.01
19		0.01 ± 0.01
20	4.27 ± 0.14 ± 0.20	
21		
22	1.66 ± 0.09 ± 0.10	
23		
24	0.69 ± 0.06 ± 0.06	
25		
26	0.24 ± 0.03 ± 0.03	
27		
28	0.05 ± 0.02 ± 0.03	

TABLE II

Parameters of the Multiplicity Distributions

	Two Jet	Single Jet
$< Nch >$	$13.02 \pm 0.03 \pm 0.50$	$6.57 \pm 0.02 \pm 0.25$
D	$3.84 \pm 0.02 \pm 0.10$	$2.71 \pm 0.02 \pm 0.06$
$\frac{<Nch>}{D}$	$3.39 \pm 0.03 \pm 0.10$	$2.42 \pm 0.03 \pm 0.10$

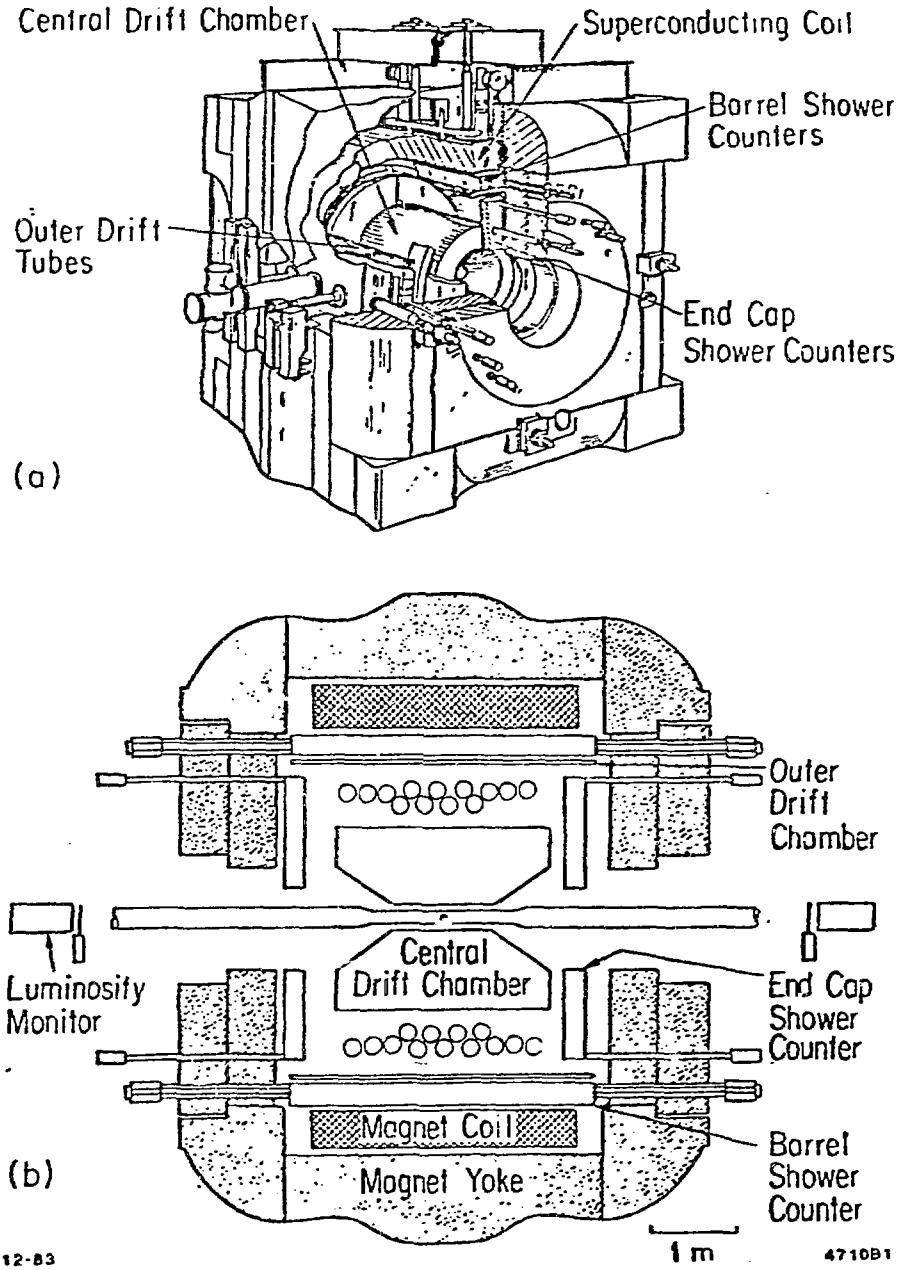

REPRODUCED FROM
BEST AVAILABLE COPY

Fig. 1

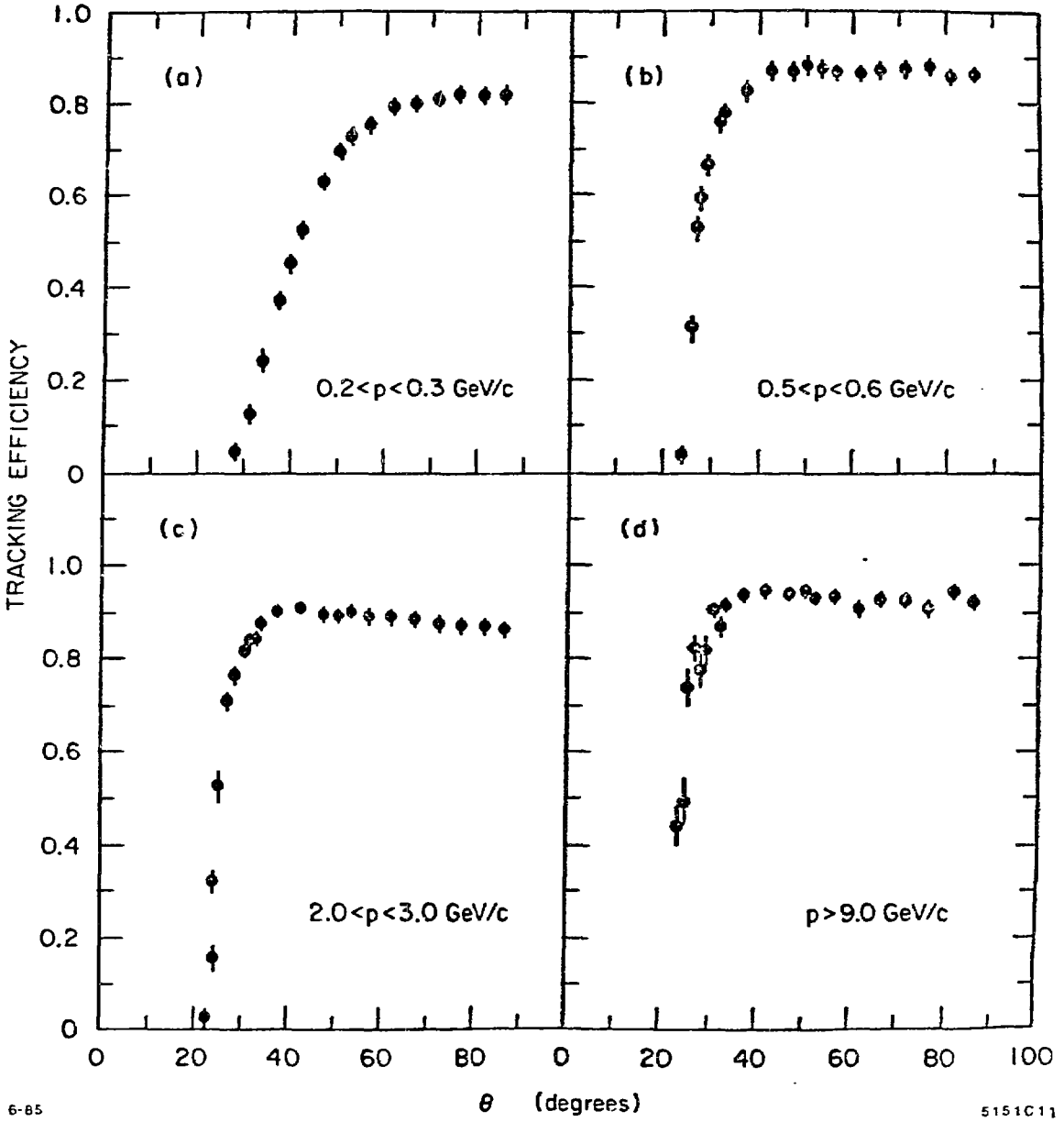
TRACKING EFFICIENCY
1.0
0.8
0.6
0.4
0.2
0
(a)
0.2<p<0.3 GeV/c
(b)
0.5<p<0.6 GeV/c
(c)
2.0<p<3.0 GeV/c
(d)
p>9.0 GeV/c
0
20
40
60
80
100
θ (degrees)
6-85
5151C11

Fig. 2

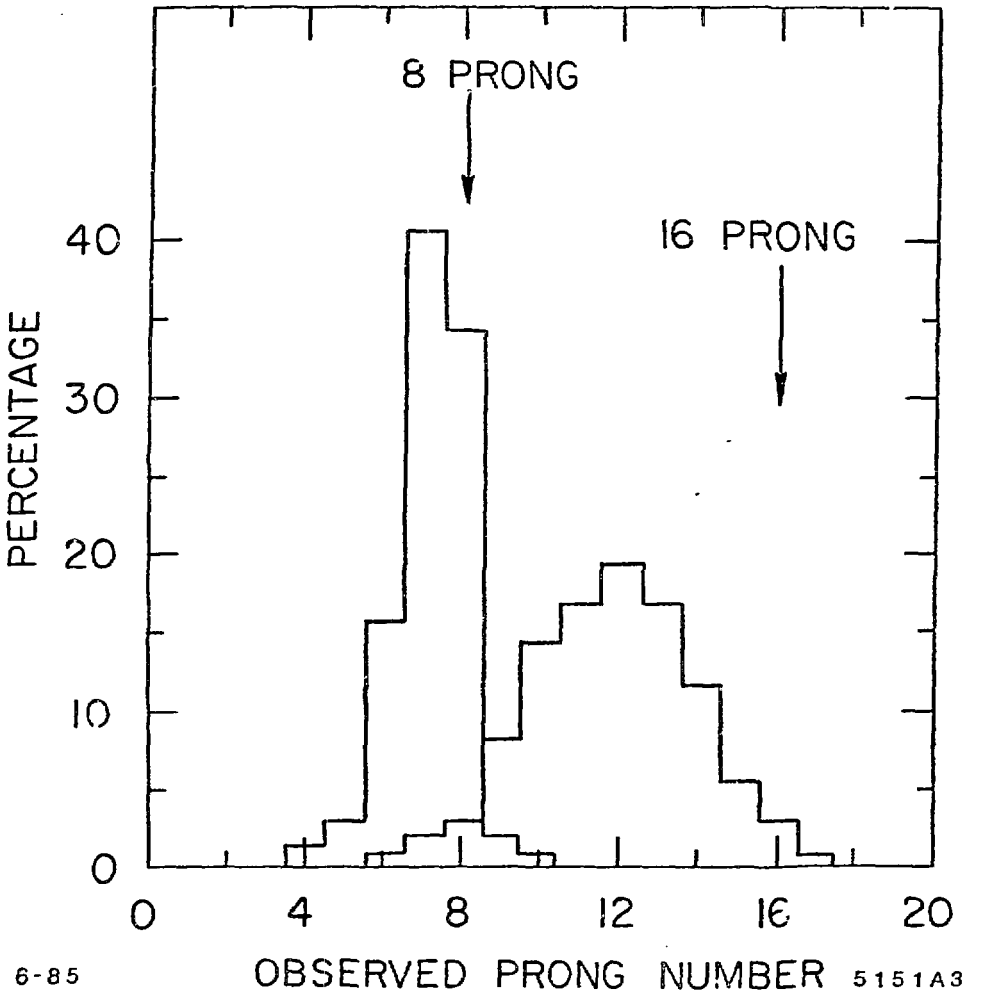
8 PRONG
16 PRONG
PERCENTAGE
40
30
20
10
0
0
4
8
12
16
20
6-85
OBSERVED PRONG NUMBER
5151A3

Fig. 3

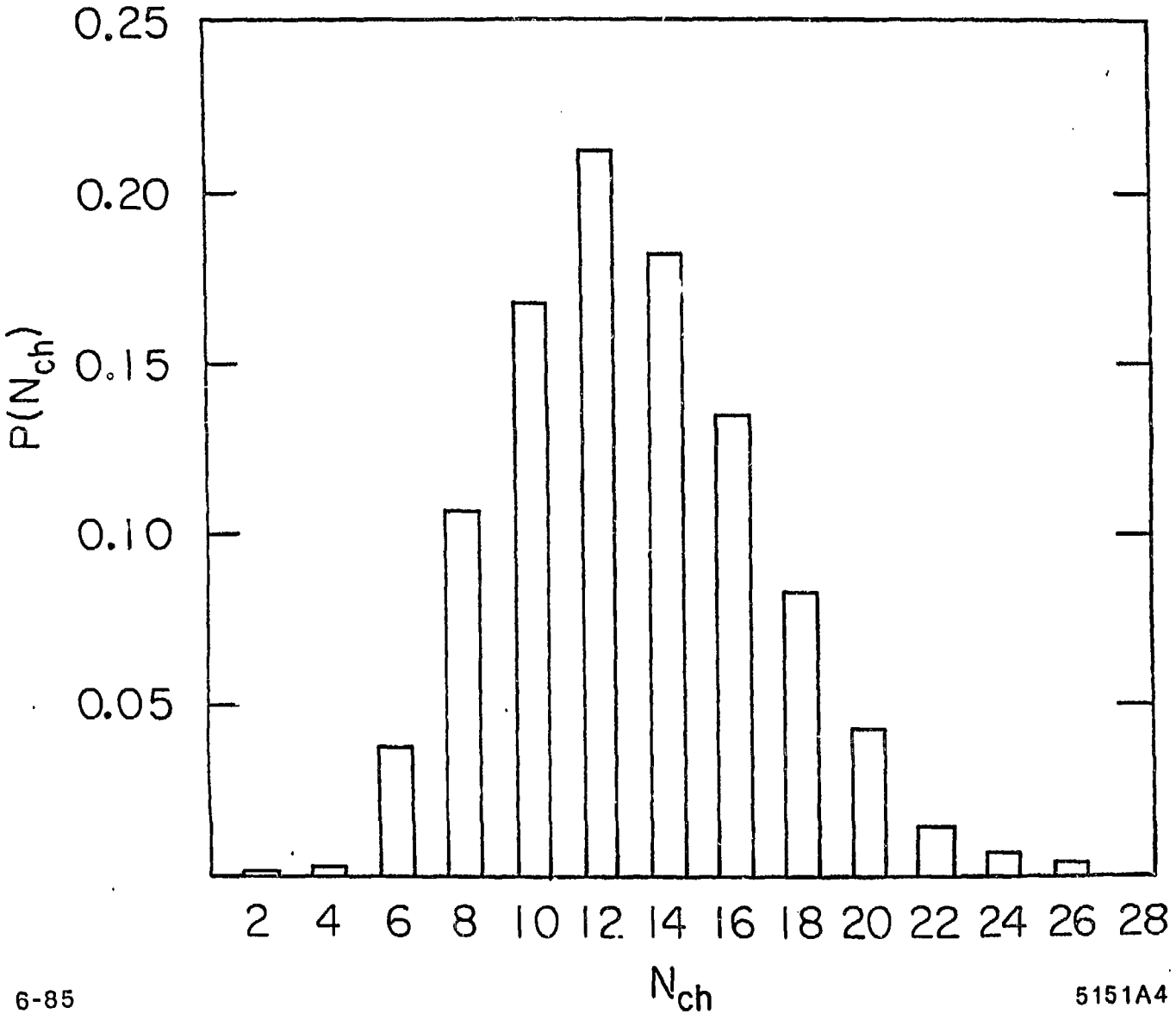

6-85

5151A4

Fig. 4

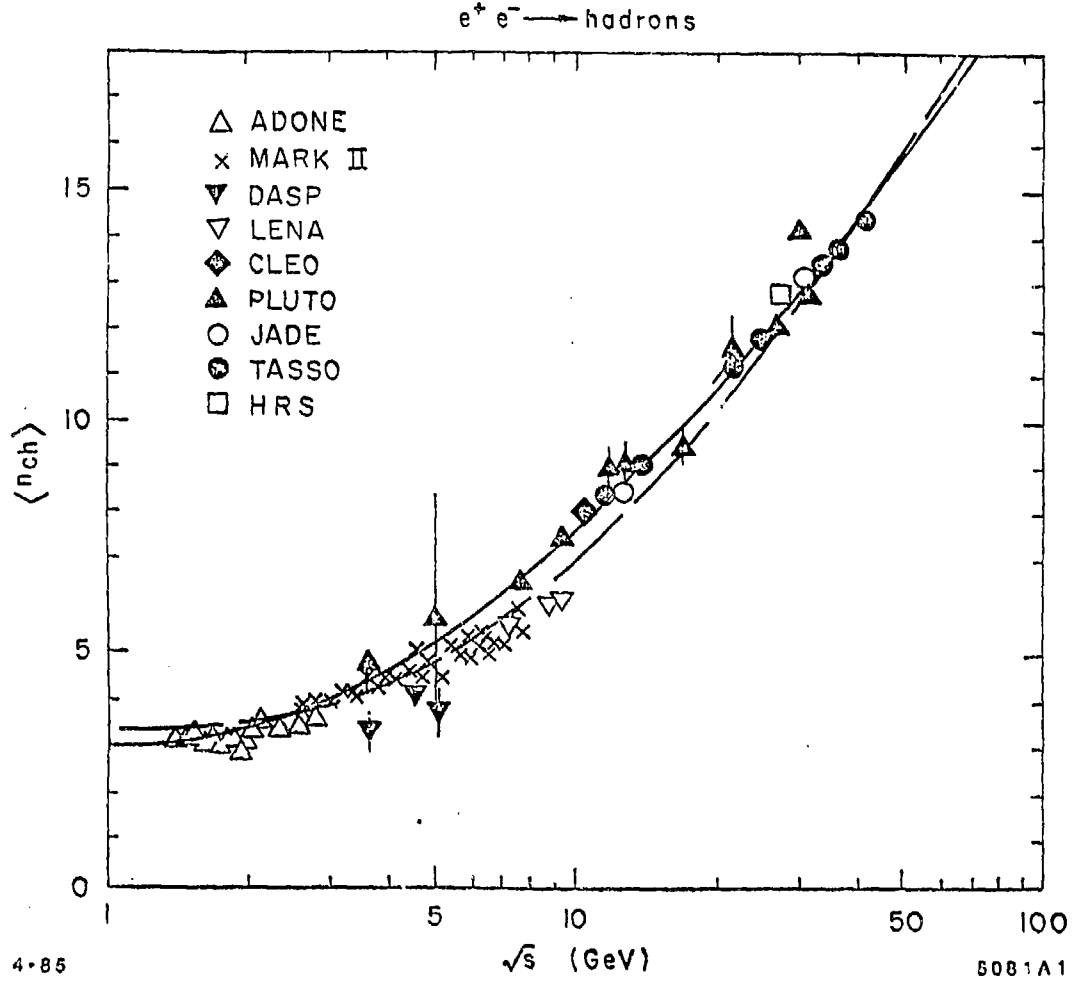
e+ e− ⟶ hadrons
ADONE
MARK II
DASP
LENA
CLEO
PLUTO
JADE
TASSO
HRS
⟨nch⟩
0
5
10
15
1
5
10
50
100
√s (GeV)
4·85
5081A1

Fig. 5a

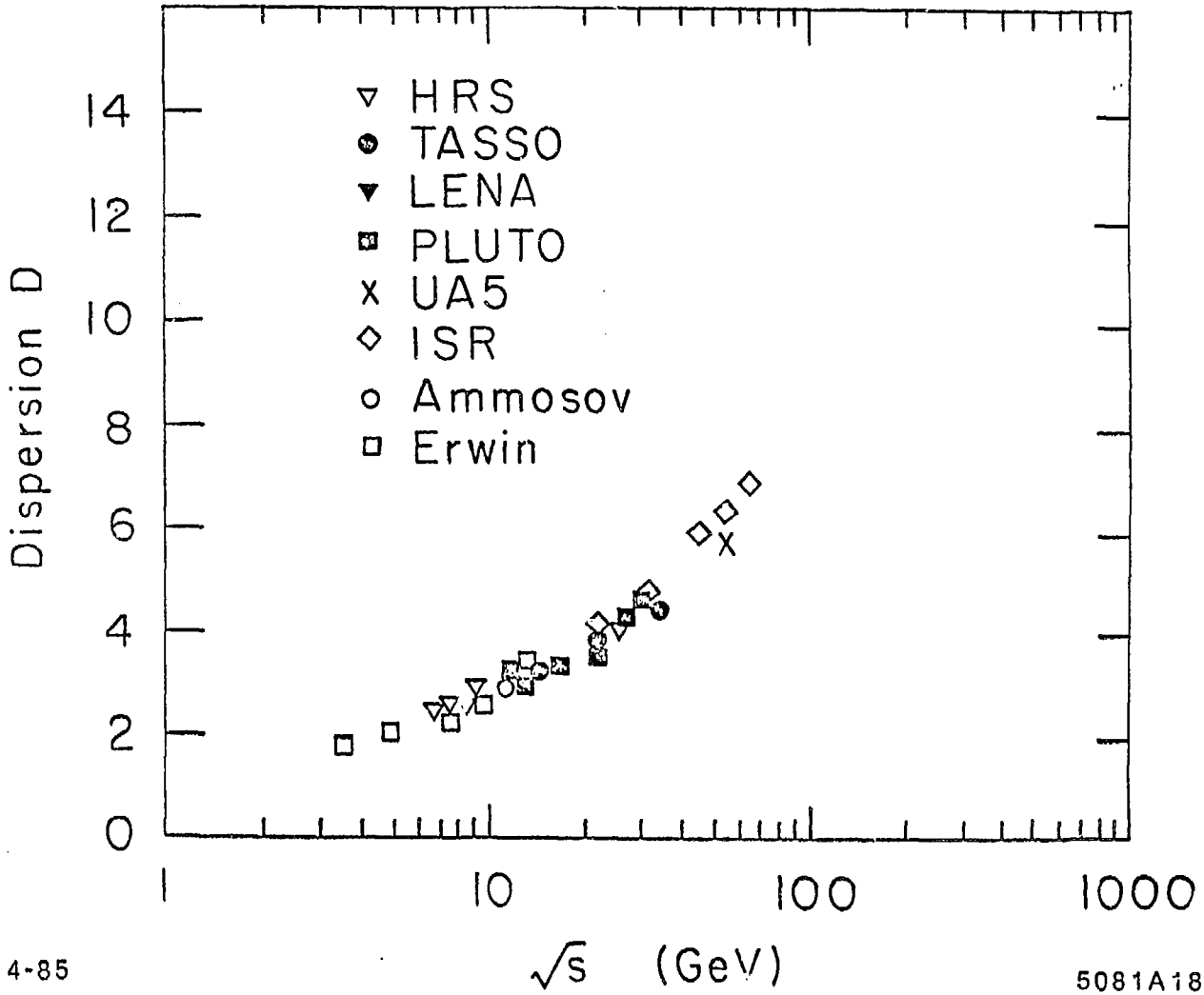
HRS
TASSO
LENA
PLUTO
UA5
ISR
Ammosov
Erwin
Dispersion D
0
2
4
6
8
10
12
14
1
10
100
1000
√s (GeV)
4-85
5081A18

Fig. 5b

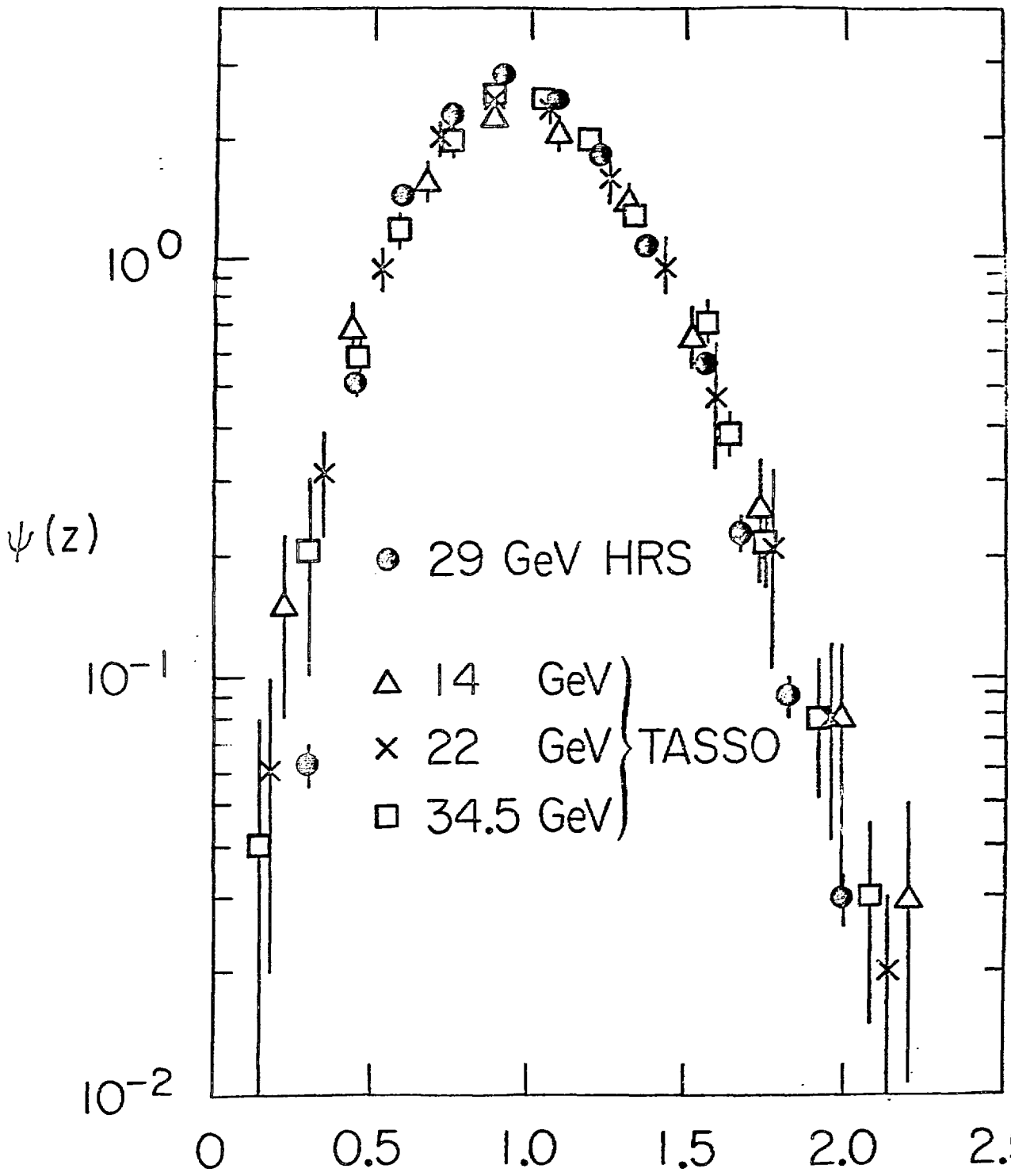
10^0
10^{-1}
10^{-2}
$\psi(z)$
29 GeV HRS
14 GeV
22 GeV
34.5 GeV
TASSO
0
0.5
1.0
1.5
2.0
2.5
Z

5151A1

Fig. 6

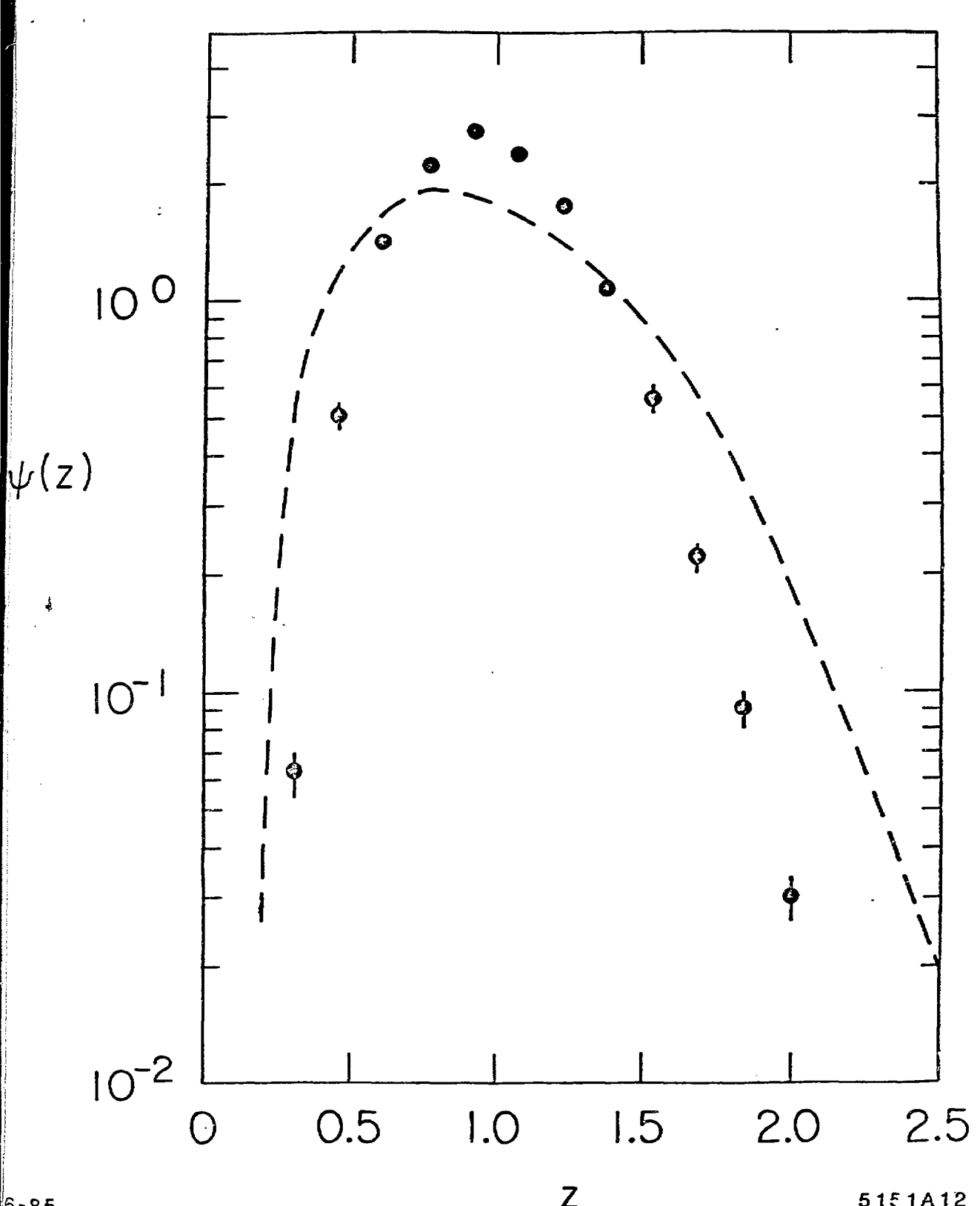

6-85

Fig. 7

5151A12

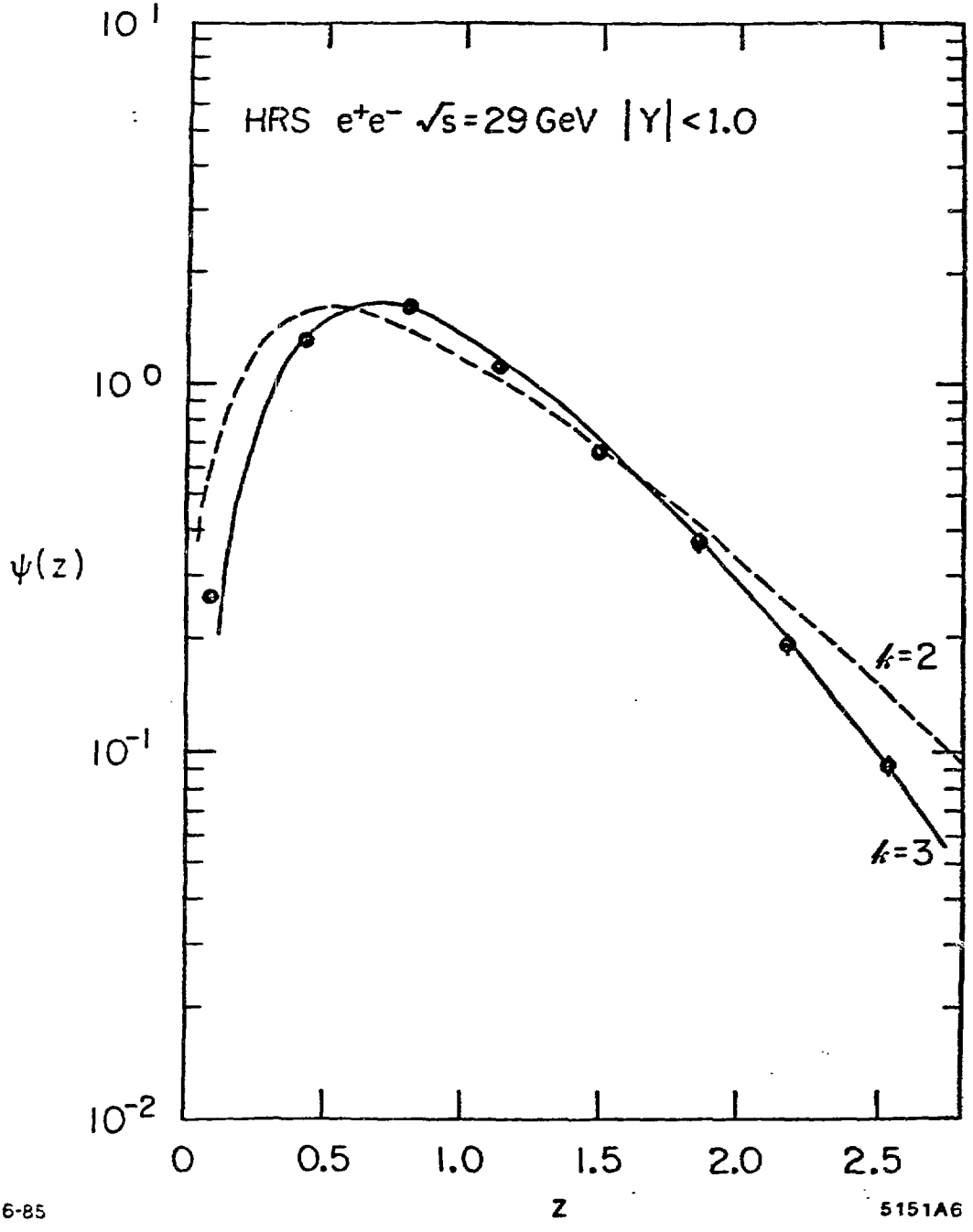
HRS e^+e^- $\sqrt{s}$=29 GeV |Y|<1.0
10^1
10^0
10^{-1}
10^{-2}
$\psi(z)$
k=2
k=3
0
0.5
1.0
1.5
2.0
2.5
z

6-85

5151A6

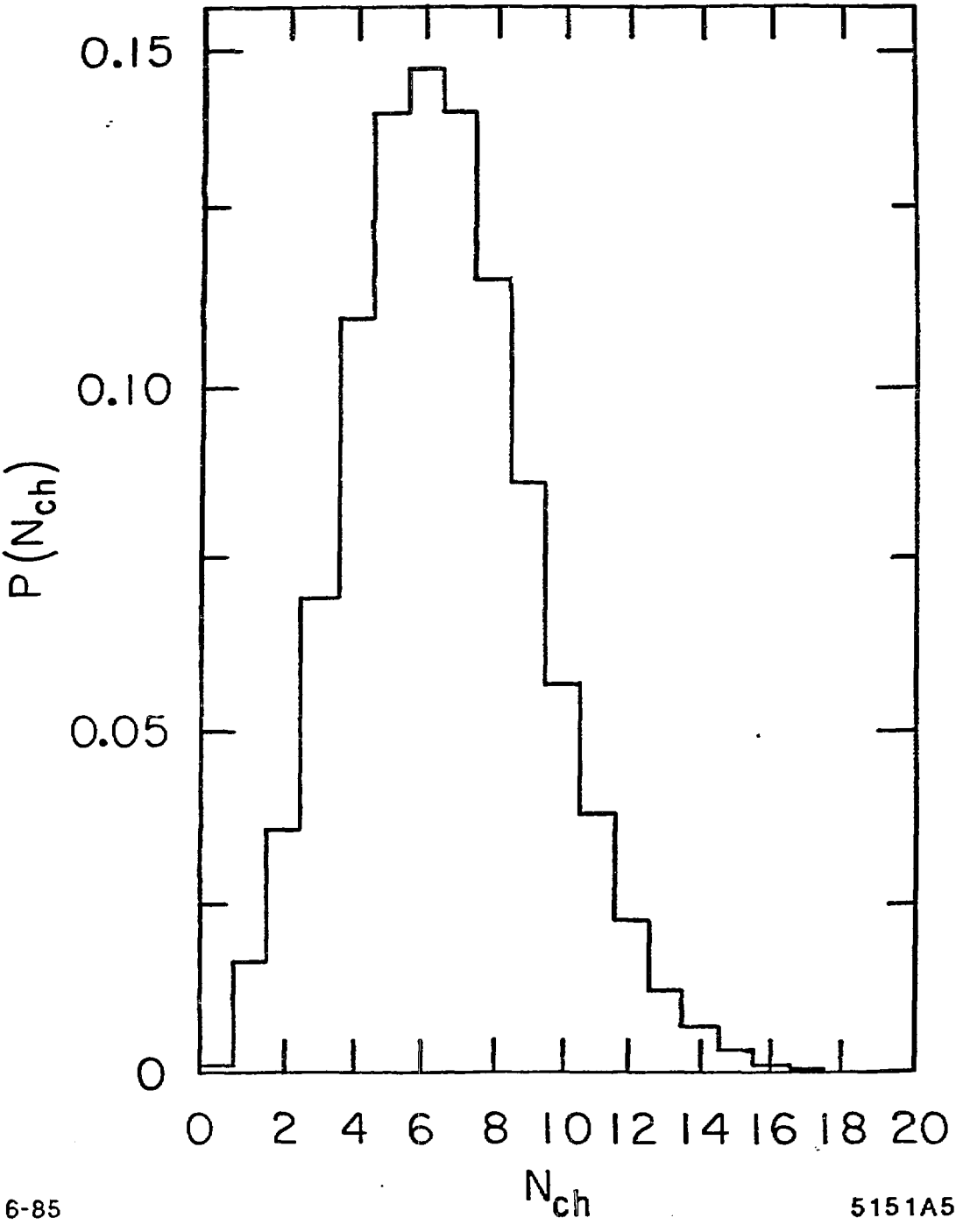

Fig. 9

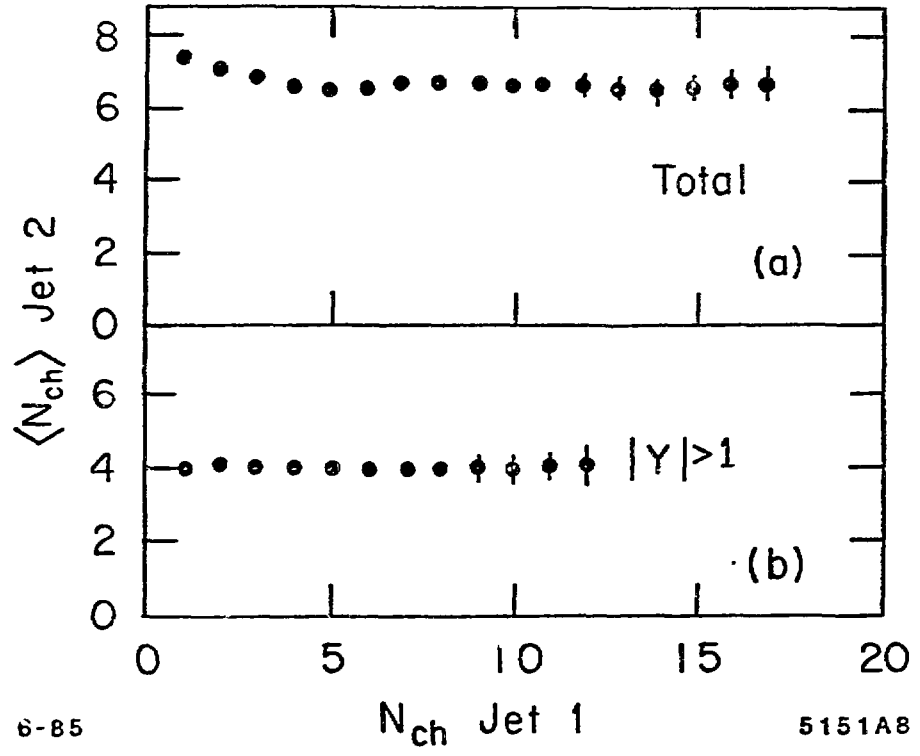

Fig. 10

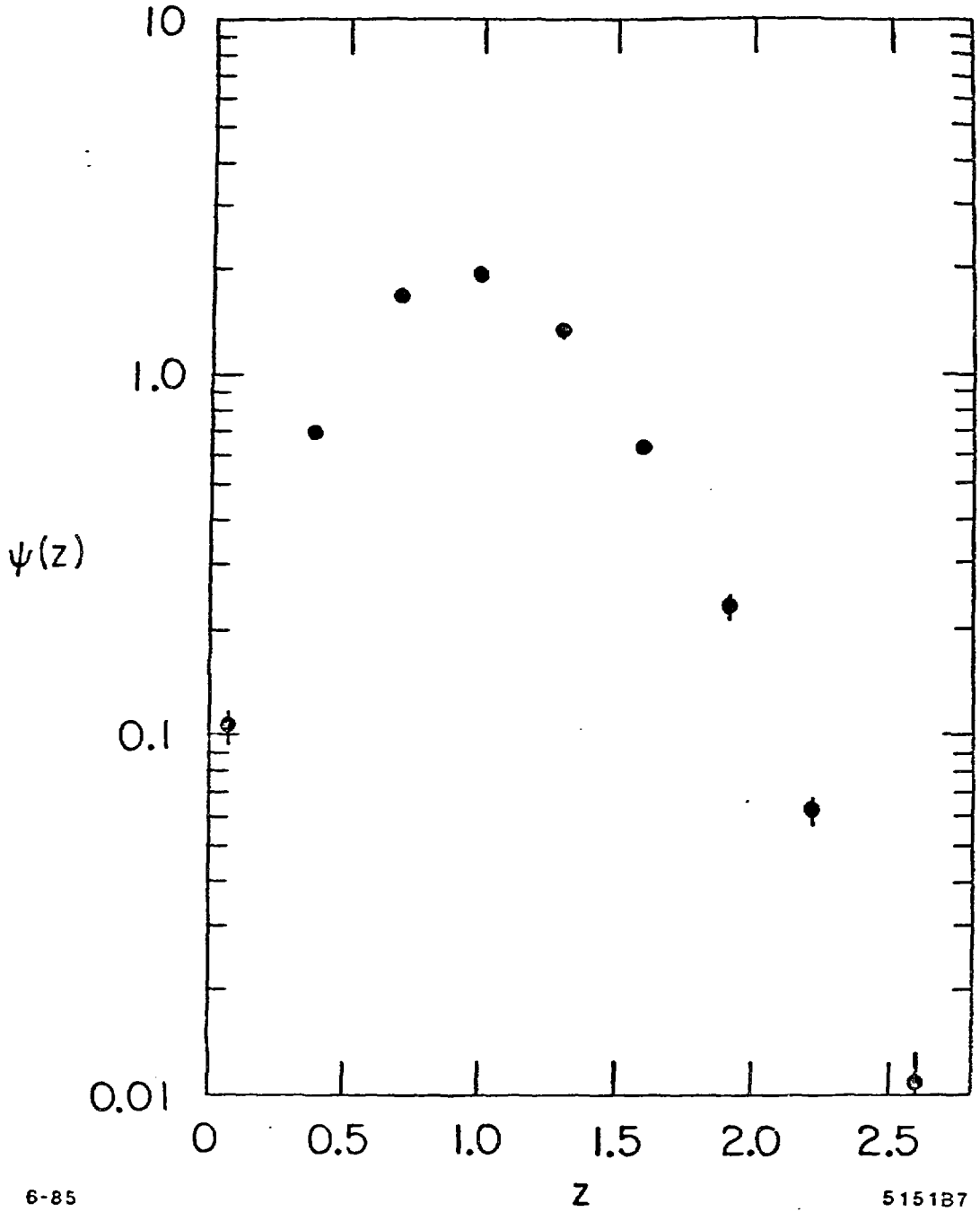

Fig. 11

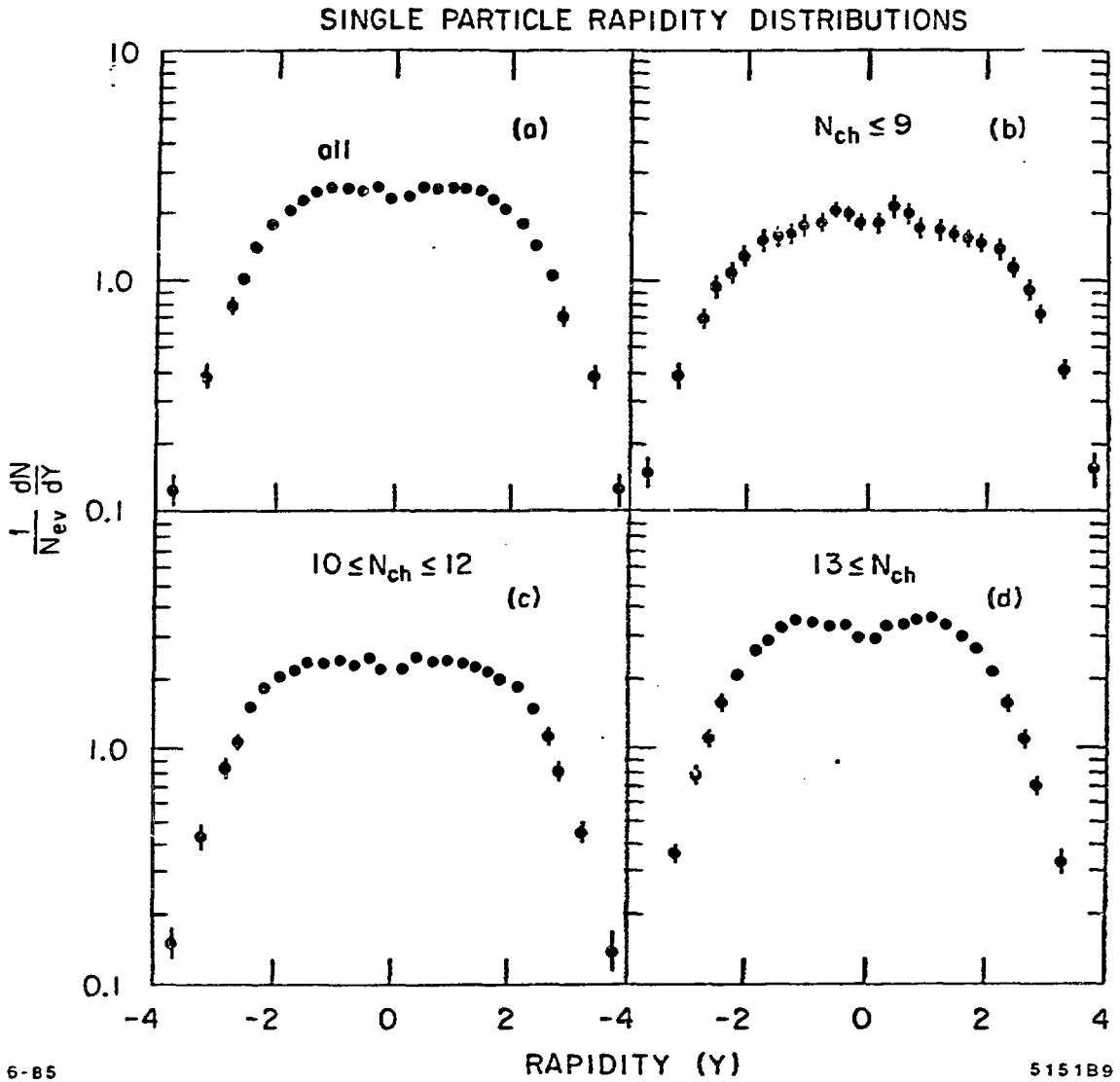
SINGLE PARTICLE RAPIDITY DISTRIBUTIONS
10
1.0
0.1
all
(a)
$N_{ch} \leq 9$
(b)
$10 \leq N_{ch} \leq 12$
(c)
$13 \leq N_{ch}$
(d)
$\frac{1}{N_{ev}} \frac{dN}{dY}$
-4
-2
0
2
-4
-2
0
2
4
RAPIDITY (Y)
6-85
5151B9

Fig. 12

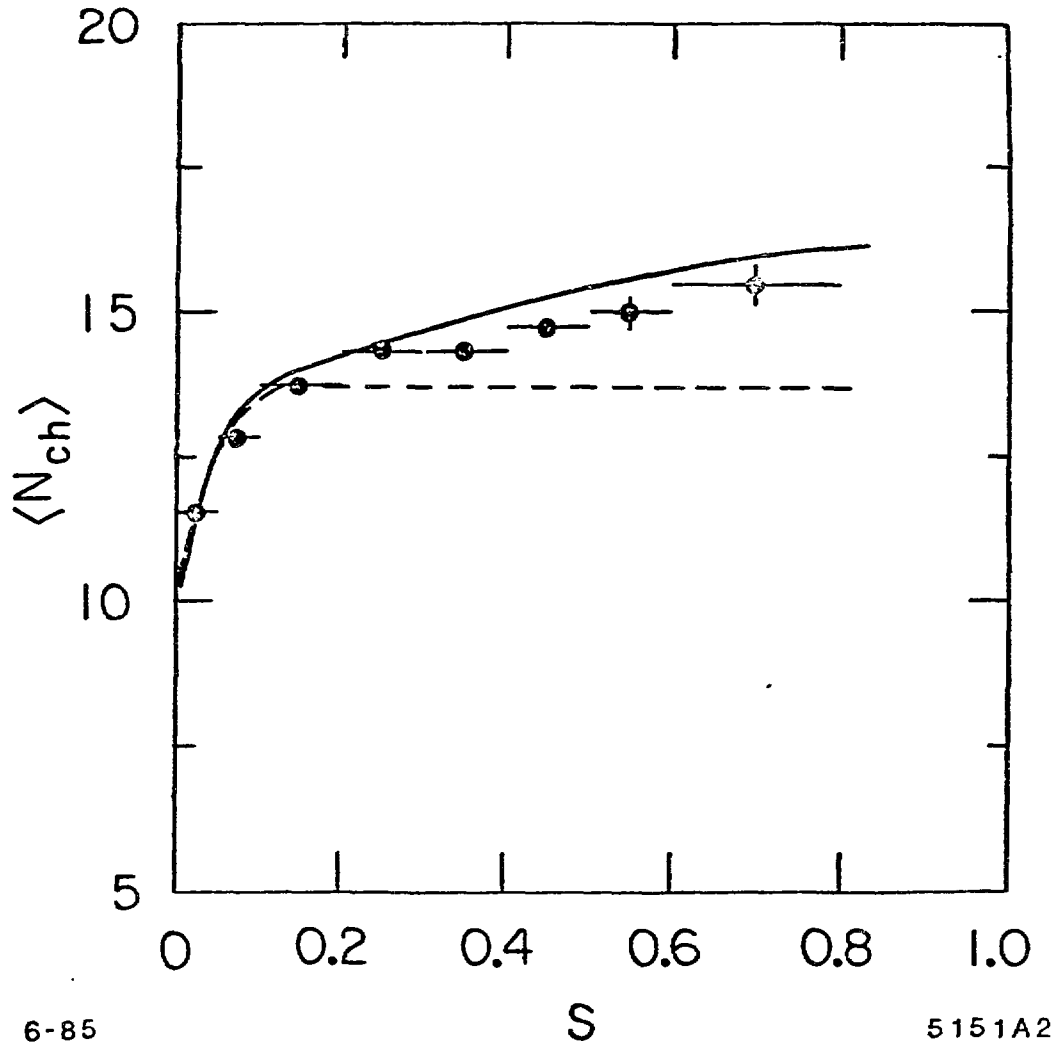

Fig. 13

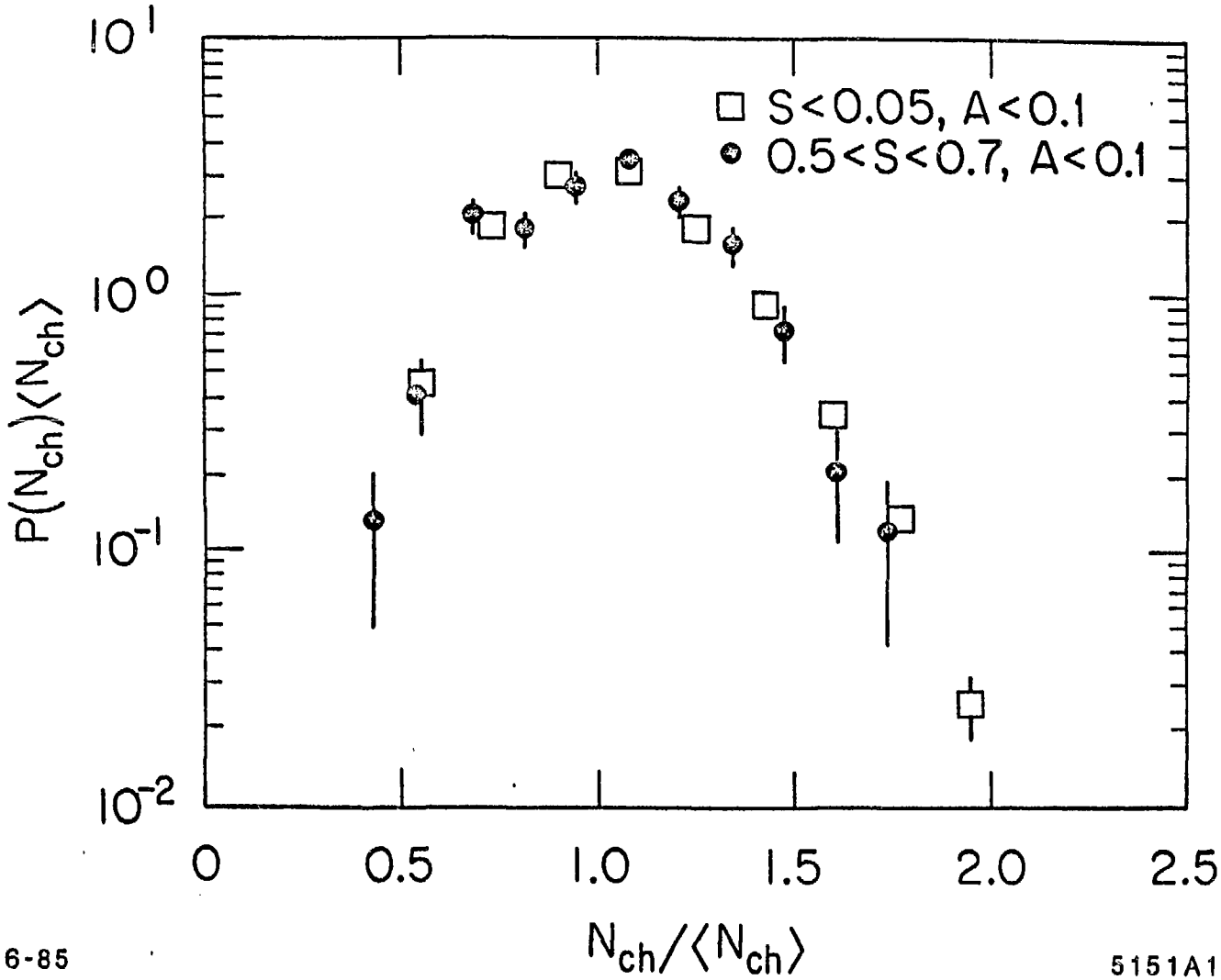
□ S<0.05, A<0.1
● 0.5<S<0.7, A<0.1
10^1
10^0
10^{-1}
10^{-2}
$P(N_{ch})\langle N_{ch}\rangle$
0
0.5
1.0
1.5
2.0
2.5
$N_{ch}/\langle N_{ch}\rangle$
6-85
5151A1

Fig. 14